Liquid Crystals
Publication details, including instructions for authors and subscription information:
http://www.informaworld.com/smpp/title~content=t713926090

Optical and dielectric properties of antiferroelectric liquid crystals and their surface effects

H. Moritake[a]; N. Shigeno[a]; M. Ozaki[a]; K. Yoshino[a]
[a] Department of Electronic Engineering, Faculty of Engineering, Osaka University, Suita, Osaka, Japan

To cite this Article Moritake, H. , Shigeno, N. , Ozaki, M. and Yoshino, K.(1993) 'Optical and dielectric properties of antiferroelectric liquid crystals and their surface effects', Liquid Crystals, 14: 5, 1283 — 1293
To link to this Article: DOI: 10.1080/02678299308026441
URL: http://dx.doi.org/10.1080/02678299308026441

LIQUID CRYSTALS, 1993, VOL. 14, NO. 5, 1283–1293

Optical and dielectric properties of antiferroelectric liquid crystals and their surface effects

by H. MORITAKE*, N. SHIGENO, M. OZAKI
and K. YOSHINO

Department of Electronic Engineering, Faculty of Engineering,
Osaka University, 2-1 Yamada-Oka, Suita, Osaka 565, Japan

A detailed study of the dielectric and optical properties of the ferroelectric liquid crystal material (*R*)-4′-(3-methoxycarbonyl-2-propoxycarbonyl)phenyl 4-(4-(*n*-octyloxy)phenyl)benzoate (3MC2PCPOPB) has been carried out. It has been found that an anomalous temperature dependence of the dielectric constant in 3MC2PCPOPB is due to the antiferroelectric and ferrielectric properties. A *T*(temperature)-*E*(electric field) phase diagram has been obtained on the basis of the apparent tilt angle measurements. In a thin cell ($<3\,\mu$m), both ferroelectric and antiferroelectric domains are simultaneously observed over a wide temperature range, and the complete antiferroelectric phase does not appear even at low temperature. A characteristic texture in which boundary focal conics are aligned parallel to a smectic layer has been observed. The movement of the zig–zag defect line caused by the application of the voltage is also observed.

1. Introduction

Since the discovery of ferroelectricity in DOBAMBC [1], a large number of ferroelectric liquid crystal materials has been synthesized and many interesting properties have been reported [2]. We have also synthesized many ferroelectric liquid crystal materials and reported novel dielectric and optical properties for them [3–5]. A few years ago, an anomalous temperature dependence of the dielectric constant in (*R*)-4′-(3-methoxycarbonyl-2-propoxycarbonyl)phenyl 4-(4-(*n*-octyloxy)phenyl)benzoate (3MC2PCPOPB) [6] was reported by us [7–9]. However, the origin of this anomaly had not been clarified at that stage of the study.

On the other hand, since the observation of antiferroelectricity in 4-(1-methylheptyloxycarbonyl)phenyl 4′-octyloxybiphenyl-4-carboxylate (MHPOBC) [10, 11], fundamental properties such as tristable switching, existence of other subphases and so on have been reported [12, 13]. From the practical point of view, some applications utilizing the tristable switching have been proposed [14, 15].

In this paper, we report anomalous behaviour of the apparent tilt angle and a novel phase sequence exhibiting antiferroelectric and ferrielectric behaviours in 3MC2PCPOPB. The dependence of antiferroelectric properties on cell thickness is also reported. Furthermore, we report polarizing microscopic textures characteristic of the antiferroelectric phase of 3MC2PCPOPB.

2. Experimental

The material used in this study was 3MC2PCPOPB [6–9]. Its molecular structure is shown in figure 1. The sample was sandwiched between two ITO (indium tin oxide) coated conducting glass plates. For the measurement of optical properties, cell surfaces

* Author for correspondence.

0267–8292/93 $10·00

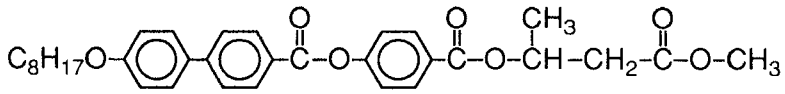

Figure 1. Molecular structure of the ferroelectric liquid crystal (*R*)-4′-(3-methoxycarbonyl-2-propoxycarbonyl)phenyl 4-[4-(*n*-octyloxy)phenyl]benzoate, 3MC2PCPOPB, used in this study.

were treated with polyimide. The cell gap was 1–25 μm, which was determined by means of capacitance measurements.

The dielectric measurements were performed with an impedance analyser (YHP, 4192). The voltage dependence of the apparent tilt angle was determined by measuring the direction of the extinction in the polarizing microscope under applied voltage. Measurement of the optical responses was performed using a polarizing microscope equipped with a photodiode detector.

3. Results and discussion

3.1. *Antiferroelectric properties of 3MC2PCPOPB*

Figure 2 shows the temperature dependence of the dielectric constant of 3MC2PCPOPB in a 25 μm thick cell. As the temperature decreases from the smectic A (S_A) phase, the dielectric constant increases at the phase transition to the chiral smectic C (S_C^*) phase. This enhancement of dielectric constant is attributed to the Goldstone mode. When the temperature decreases further, the dielectric constant is suppressed and becomes nearly the same as that in the S_A phase. This suppression may be caused by disappearance of the contribution of the Goldstone mode [16].

Figure 3 shows the voltage dependences of the apparent tilt angle in the temperature range in which the contribution of the Goldstone mode is suppressed as previously mentioned. The apparent tilt angle is defined as the angle between the layer normal and the extinction direction in the polarizing microscope. As is evident from figure 3 (*a*), the apparent tilt angle indicates three stable states at higher temperature (107°C). One state in which the extinction direction is parallel to the layer normal is

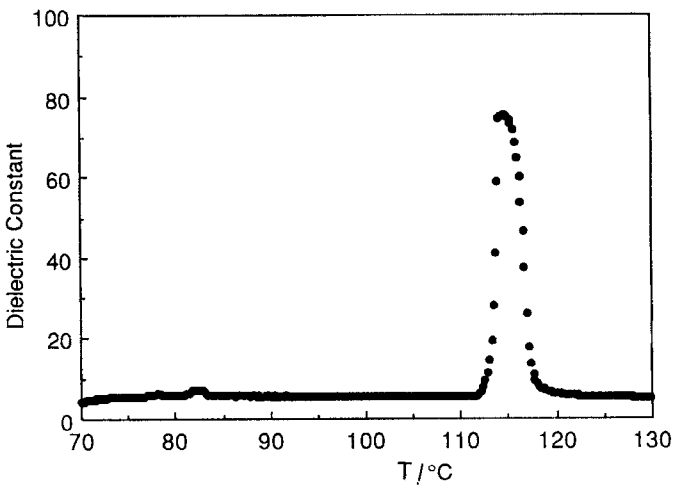

Figure 2. Temperature dependence of the dielectric constant in a 25 μm thick cell of 3MC2PCPOPB at 1000 Hz.

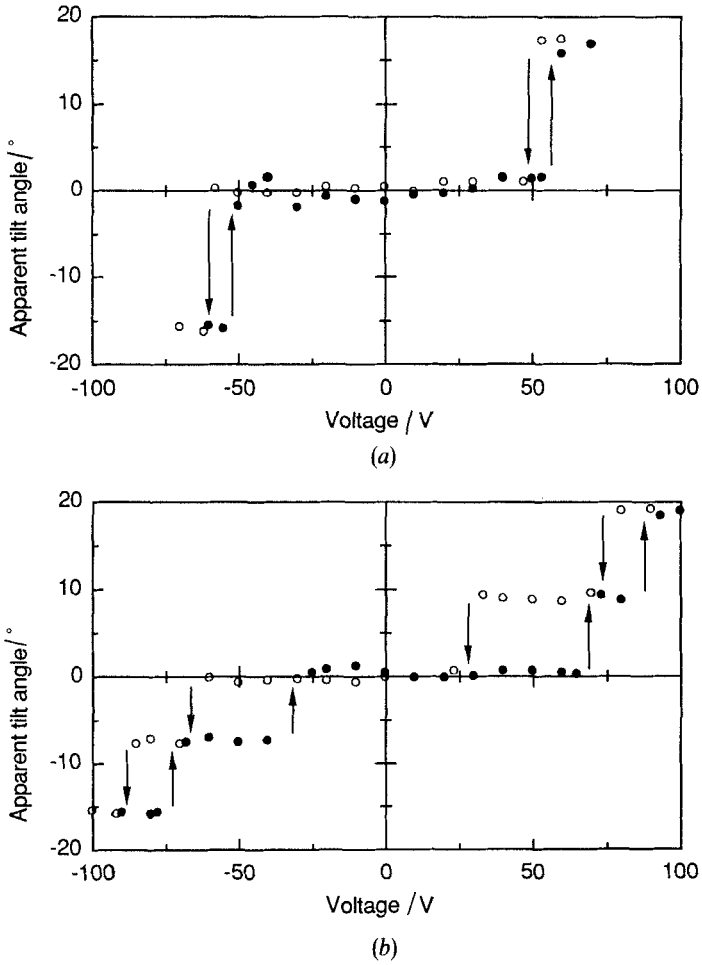

Figure 3. Voltage dependences of apparent tilt angle in a cell 6 μm thick in the $S^*_{C_A}$ phase (*a*) at 107°C and (*b*) at 95°C.

observed at low applied voltage, and two other states which correspond to the uniform state are observed at high applied voltages. This switching phenomenon may be the same as the tristable switching observed for antiferroelectric liquid crystals such as MHPOBC [10]. This agrees with the disappearance of the Goldstone mode, i.e. the suppression of the dielectric constant. Consequently, the temperature range in which the Goldstone mode disappears in 3MC2PCPOPB is attributed to the chiral smectic C_A ($S^*_{C_A}$) phase.

The voltage dependence of the apparent tilt angle at a lower temperature (95°C) is shown in figure 3 (*b*). As is evident from this figure, two other states in which the apparent tilt angle is half of that in the bistable ferroelectric states were observed at intermediate applied voltage, in addition to the three states shown in figure 3 (*a*). In other words, five stable states of the apparent tilt angle were clearly recognized.

Figure 4 shows the optical responses with triangular waves at various temperatures. The transmission intensity indicates three and five stable states in figures 4 (*a*) and (*b*),

respectively. They correspond to the voltage dependences of apparent tilt angle in figure 3. When the temperature decreased further to 86°C, the transmission intensity showed four stable states as shown in figure 4 (*c*).

Novel phases such as the chiral smectic C_γ ($S^*_{C_\gamma}$) phase have been reported for MHPOBC, and the $S^*_{C_\gamma}$ phase was interpreted to be a ferrielectric phase [12]. In the $S^*_{C_\gamma}$ phase, the voltage dependence of the transmittance shows four stable states. By analogy with the $S^*_{C_\gamma}$ phase of MHPOBC, the lower temperature range in 3MC2PCPOPB may be interpreted as relating to the $S^*_{C_\gamma}$ phase.

In MHPOBC, the $S^*_{C_\gamma}$ phase, in which the voltage dependence of the transmittance indicates four stable states, appears between the S^*_C and $S^*_{C_A}$ phases, and the $S^*_{C_\gamma}$–$S^*_{C_A}$ transition temperature shifts toward lower temperatures with increasing applied field. Therefore, just below the S^*_C phase, four stable states, i.e. ferroelectric S^*_C–ferrielectric $S^*_{C_\gamma}$–$S^*_{C_\gamma}$–S^*_C, were observed, and then, as the temperature decreased further, five stable states arise from the field-induced phase transition, i.e. S^*_C–$S^*_{C_\gamma}$–antiferroelectric $S^*_{C_A}$–$S^*_{C_\gamma}$–S^*_C, were observed [17].

On the other hand, in 3MC2PCPOPB the S^*_C phase directly changes into the $S^*_{C_A}$ phase and the stable states of the transmission intensity (three, five and four states) appear, sequentially, as shown in figure 4. This sequential change can be explained as follows. The $S^*_{C_\gamma}$ phase exists below the $S^*_{C_A}$ phase [18] and the $S^*_{C_A}$–$S^*_{C_\gamma}$ transition temperature shifts toward higher temperatures with increasing applied field. Therefore, in the lower temperature range of the $S^*_{C_A}$ phase, five stable states arising from the field-induced phase transition, i.e. S^*_C–$S^*_{C_\gamma}$–$S^*_{C_A}$–$S^*_{C_\gamma}$–S^*_C, were observed. And in the $S^*_{C_\gamma}$ phase, four stable states originated from the field-induced phase transition, i.e. S^*_C–$S^*_{C_\gamma}$–$S^*_{C_\gamma}$–S^*_C

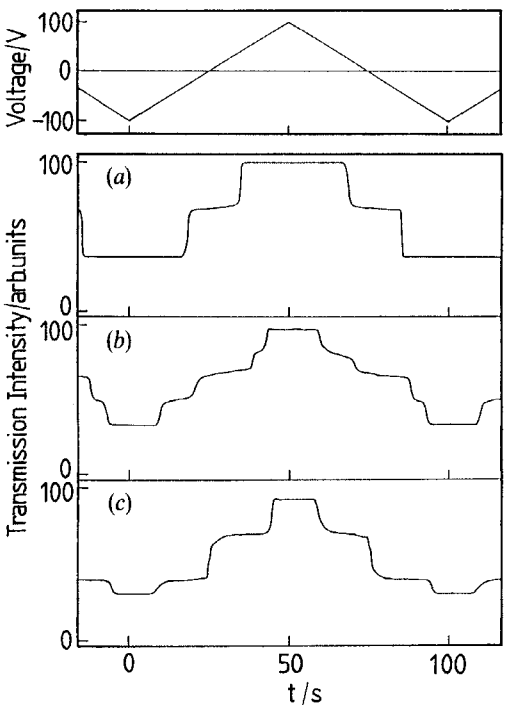

Figure 4. Transmission intensity changes with a triangular voltage wave. (*a*) and (*b*) are for the $S^*_{C_A}$ phase ((*a*) at 106°C, (*b*) at 92°C). (*c*) is for the $S^*_{C_\gamma}$ phase at 86°C.

appeared. Then the voltage dependences of apparent tilt angle (see figure 3) and the optical responses under triangular waves (see figure 4) may be attributed to this novel phase sequence in this compound which has never been reported.

Figure 5 shows a temperature–electric field phase diagram of 3MC2PCPOPB obtained on the basis of apparent tilt angle measurements. With decreasing temperature from the S_C^*–$S_{C_A}^*$ transition temperature (111°C), the transition field between the S_C^* and $S_{C_A}^*$ phases monotonically increases. In this temperature range (111–100°C), only one transition field was observed, which corresponds to three stable states of the apparent tilt angle as shown in figure 3 (*a*). Below about 100°C, the transition field was divided into two fields. One is the transition field between the $S_{C_A}^*$ and $S_{C_\gamma}^*$ phases, and the other is the transition field between the $S_{C_\gamma}^*$ and S_C^* phases. The former and latter fields are defined as E_1 and E_2, respectively. Below 90°C the field E_1 decreased rapidly toward zero and disappeared with the phase transition to the $S_{C_\gamma}^*$ phase. On the contrary, in this temperature range (below 88°C), the transition field E_2 could be observed in the same manner as that at the higher temperature and the transmittance indicated four stable states.

The dielectric constant in the $S_{C_\gamma}^*$ phase is expected to increase compared with that in the $S_{C_A}^*$ phase. But in 3MC2PCPOPB, the dielectric constant in the $S_{C_\gamma}^*$ phase remained the same as that in the $S_{C_A}^*$ phase, as shown in figure 2. To clarify the origin of this phenomenon, the polarizing microscopic observation under zero electric field was carried out. If the direction of one of the crossed polarizers is set parallel to the layer normal, an extinction is observed in the S_A phase. As the temperature decreases from the S_A phase, maintaining the direction of the polarizers, the extinction once again disappears in the S_C^* phase and is obtained again in the $S_{C_A}^*$ phase. When the temperature decreases further, in spite of the transition into the $S_{C_\gamma}^*$ phase (< 88°C), the extinction did not disappear and remained the same as for the $S_{C_A}^*$ phase. In other words, the apparent tilt angle with no field is zero in the $S_{C_\gamma}^*$ phase of 3MC2PCPOPB. However, in the measurement of the voltage dependence of the apparent tilt angle and the transmission intensity, the apparent tilt direction of the molecules does not stably orient to the layer normal under low field, which indicates the occurrence of the $S_{C_\gamma}^*$ phase. On condition that a field has not been exerted, the $S_{C_A}^*$ phase remains at lower

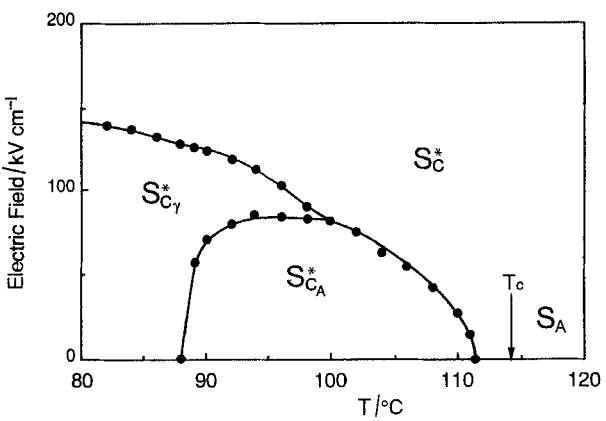

Figure 5. T–E phase diagram of 3MC2PCPOPB obtained on the basis of apparent tilt angle measurements in a 6 μm thick cell. T_c is the phase transition temperature between the S_A and S_C^* phases in the absence of the electric field.

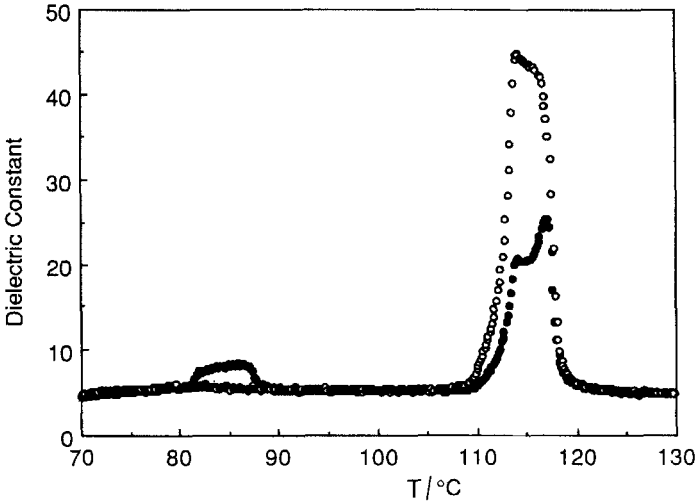

Figure 6. Temperature dependence of the dielectric constant after the application of the bias voltage in a 6 μm thick cell of 3MC2PCPOPB (closed circles) at 1000 Hz. Open circles denote the dielectric constant of the virgin sample.

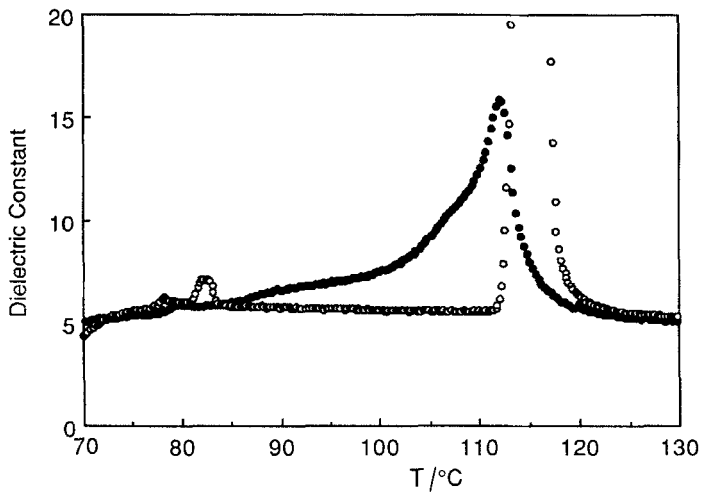

Figure 7. Temperature dependence of the dielectric constant in a 1 μm (closed circles) and 25 μm (open circles) cell of 3MC2PCPOPB at 1000 Hz.

temperature and the $S^*_{C_\gamma}$ phase does not appear. Once the electric field is applied, the $S^*_{C_\gamma}$ phase appears. Consequently, the field induced phase transition from the $S^*_{C_A}$ phase to the $S^*_{C_\gamma}$ phase may occur.

In order to investigate the field induced transition, dielectric measurements after the application of the field were performed. Figure 6 shows the temperature dependence of the dielectric constant after applying the field (closed circles). The dc bias voltage (35 V) was applied before the measurement of the dielectric constant at each temperature. The dielectric constant without field is also shown in figure 6 (open circles). The dielectric constant in the S^*_C phase was suppressed compared with that with no field. This suppression of the dielectric constant is attributed to the suppression of the

contribution of the Goldstone mode, because of the remaining effect of applying the field. It should be noted that the dielectric constant in the $S^*_{C_\gamma}$ phase increases when it was measured after the voltage application. From this result, it is confirmed that the phase transition from the $S^*_{C_A}$ phase to the $S^*_{C_\gamma}$ phase occurs after the field application.

3.2. *Dependence of antiferroelectric properties on cell thickness*

Figure 7 shows the temperature dependence of the dielectric constant of 3MC2PCPOPB in a 1 μm thick cell (closed circles). The dielectric constant of a 25 μm thick cell is also shown in figure 7 (open circles). The dielectric constant in the S^*_C phase in the 1 μm thick cell was suppressed compared with that of the 25 μm thick cell shown in figure 2. This suppression of the dielectric constant in the thin cell is attributed to a surface effect which suppresses the contribution of the Goldstone mode [16]. It should be noted that the dielectric constant does not decrease rapidly even after the phase transition from the S^*_C phase to the $S^*_{C_A}$ phase and does not fall to the same level as that in the S_A phase.

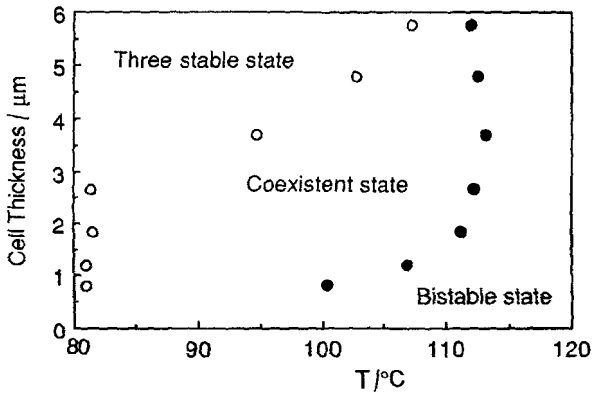

Figure 8. The cell thickness dependence of the S^*_C–$S^*_{C_A}$ transition temperature.

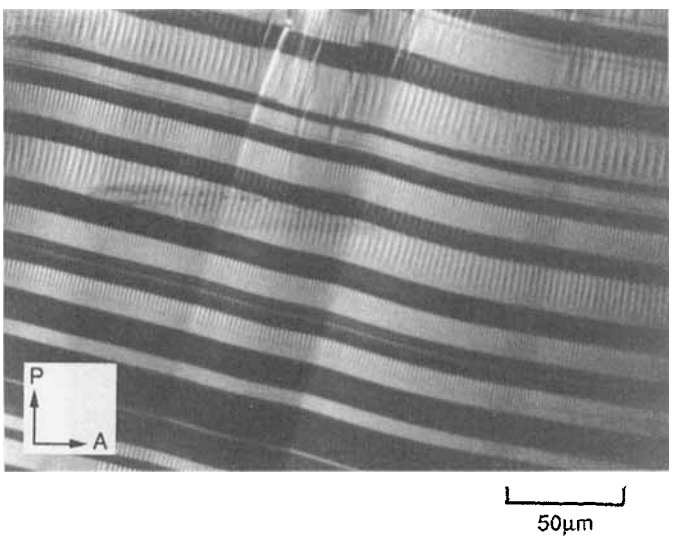

Figure 9. Micrograph of a homogeneously aligned cell of 3MC2PCPOPB just below the phase transition temperature from the S^*_C phase to the $S^*_{C_A}$ phase. The dark and the white stripes represent the ferroelectric and antiferroelectric domains, respectively.

The polarizing microscopic observation was carried out using a thin cell (less than 1 μm). In the thin cell, although the S_C^*–$S_{C_A}^*$ transition temperature shifts toward lower temperatures, below that transition temperature antiferroelectric stripe domains grow along the smectic layer in the same manner as in a thick cell. However, with a further decrease of temperature, both ferroelectric and antiferroelectric domains remain throughout the $S_{C_A}^*$ phase in the absence of the electric field. In other words, the S_C^* and $S_{C_A}^*$ phases are simultaneously observed even at the low temperature at which only the $S_{C_A}^*$ phase is shown in a thick cell [19]. Therefore, the enhancement of the dielectric constant shown in figure 7 may be attributed to the coexistence of the S_C^* and $S_{C_A}^*$ phases.

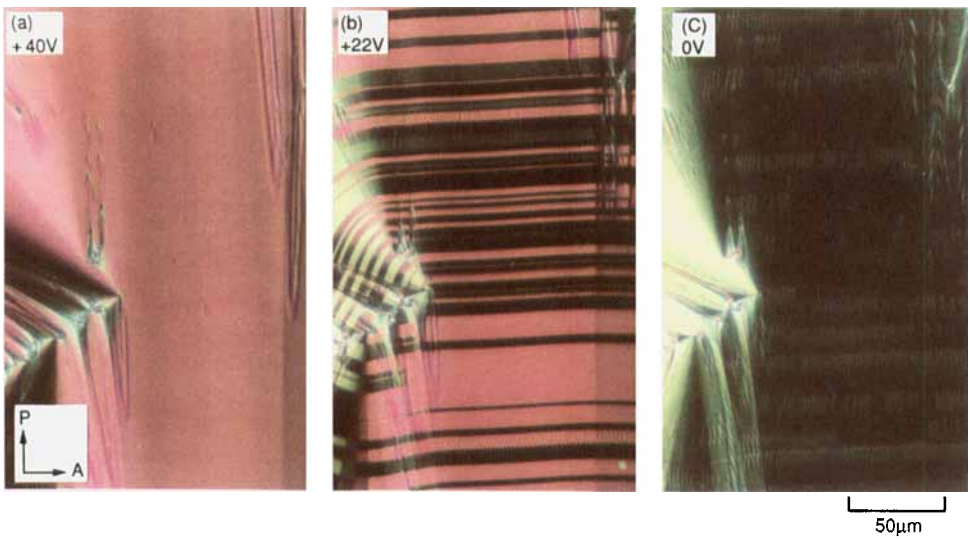

Figure 10. Micrographs of a homogeneously aligned cell of 3MC2PCPOPB in the antiferroelectric phase ($S_{C_A}^*$, 103·5°C) as a function of applied voltage at (*a*) 40 V, (*b*) 22 V and (*c*) 0 V.

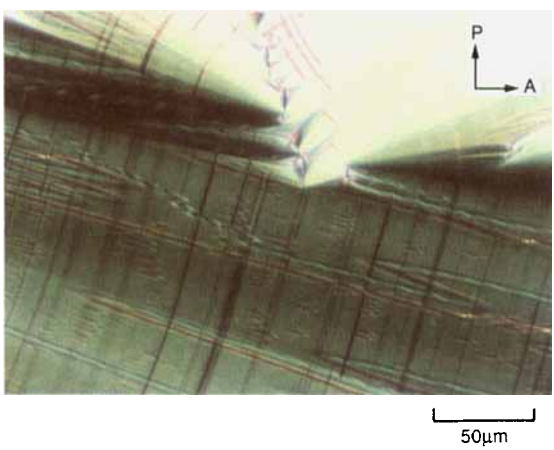

Figure 11. Micrograph of a homogeneously aligned cell of 3MC2PCPOPB at a lower temperature (95°C) in the antiferroelectric phase. The applied voltage is 29 V. The same part of the sample cell as that in figure 10 is shown.

Figure 8 shows the cell thickness dependence of the S_C^*–$S_{C_A}^*$ transition temperature. In this figure, two states (bistable and three stable states) and one coexistent state are distinguished. With decreasing cell thickness, the temperature range of the coexistent state expands and shifts toward the lower temperature. The ratio of the areas of three stable domains to bistable domains gradually increases with decreasing temperature. In a thin cell, less than 3 μm in thickness, the temperature range with complete three stable states disappears even in the entire $S_{C_A}^*$ phase and ferroelectric and antiferroelectric domains coexist.

3.3. *Characteristic texture in antiferroelectric phase*

The polarizing microscopic observation was carried out using a thin cell (2–6 μm in thickness). Just below the transition temperature from the S_C^* phase to the $S_{C_A}^*$ phase, both the ferroelectric and antiferroelectric domains coexist even in the absence of the electric field. Figure 9 shows the polarizing micrograph just below the S_C^*–$S_{C_A}^*$

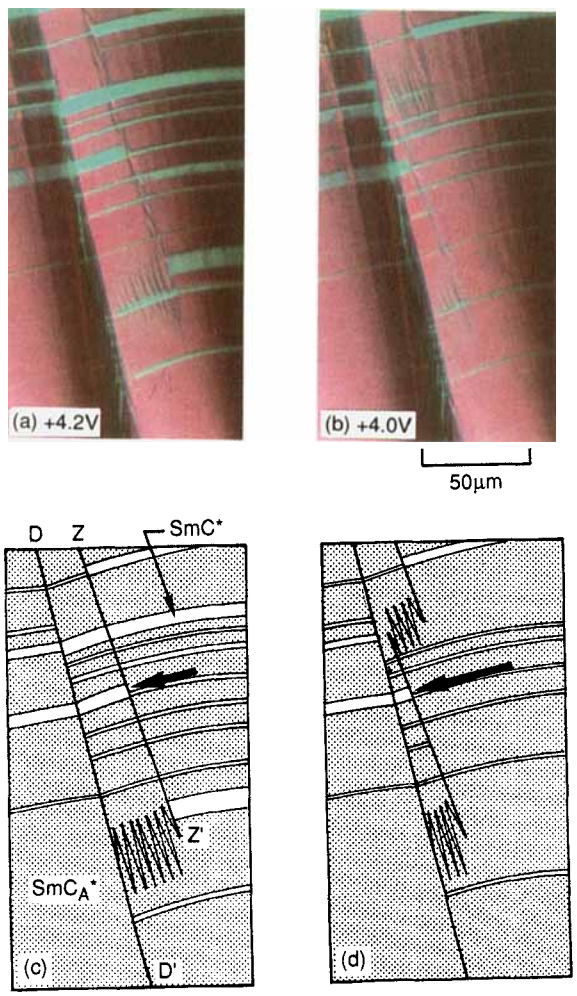

Figure 12. Micrographs of a homogeneously aligned cell of 3MC2PCPOPB in the antiferroelectric phase ($S_{C_A}^*$, 103·5°C) as a function of applied voltage, (*a*) at 4·2 V, (*b*) at 4·0 V. (*c*) and (*d*) illustrate the micrographs (*a*) and (*b*), respectively, by way of explanation of the motion of the zig–zag defect line (Z–Z').

transition temperature. The white and the dark regions in the photograph correspond to antiferroelectric and ferroelectric domains, respectively. The extinction direction of the antiferroelectric domain is perpendicular to the smectic layers. It should be noted that the periodic stripes aligned along the smectic layer at equal distances are observed. Although these periodic stripes were observed at the boundary between ferroelectric and antiferroelectric domains, no stripes were observed in the ferroelectric state induced by the application of the electric field.

Figure 10 shows the polarizing micrographs at various applied voltages in the $S^*_{C_A}$ phase (103·5°C). At this temperature, only the antiferroelectric state was observed in the absence of the electric field. As mentioned above, the transition from antiferroelectric state to ferroelectric state is caused by the application of the voltage. Figure 10 (*a*) shows the microscopic texture in the ferroelectric state induced by voltage application. In this state, the periodically aligned patterns shown in figure 9 were not observed. With decreasing voltage, the ferroelectric state turns into the antiferroelectric state accompanied by the growth of the antiferroelectric stripe domains (dark stripes shown in figure 10 (*b*)). As the antiferroelectric domains grow, new periodic patterns shown in figure 9 appear at the boundary between ferroelectric and antiferroelectric domains. When the complete antiferroelectric state was established without field, periodically aligned patterns remain in spite of the disappearance of the stripe domains as shown in figure 10 (*c*).

To clarify the characteristic pattern, microscopic observations at lower temperatures were carried out. Figure 11 shows a micrograph at 95°C. The zig–zag defect lines are observed. The appearance of these zig–zag defect lines suggests the formation of the chevron layer structure [20]. Although the patterns shown in figure 10 were observed, they were randomly distributed. The patterns in two regions separated by the zig–zag defect line are arranged in the opposite direction. Therefore, the patterns which align at the boundary between the ferroelectric and antiferroelectric domains must be focal-conic defects due to the chevron layer structure [21].

Figure 12 (*a*) and (*b*) show polarizing micrographs at 103·5°C as a function of applied voltage. With decreasing voltage, the ferroelectric state turns into the antiferroelectric state accompanying the growth of the stripe domain. It should be noted that, following the growth of the stripe domains, the zig–zag defect line gradually moves. For convenience, the schematic explanation of this movement is illustrated in figure 12 (*c*) and (*d*). The growth of the stripe domains of the antiferroelectric state towards the defect line D–D′ is obstructed by the zig–zag defect line Z–Z′. As the voltage decreases, the further growth of the stripe domains causes the zig–zag defect line to move as shown in figure 12 (*d*). The zig–zag defect line moves more quickly and dynamically at the higher temperatures.

4. Summary

Dielectric and optical properties for 3MC2PCPOPB were studied in detail. The anomalous dielectric property in 3MC2PCPOPB was interpreted to be due to the antiferroelectric and ferrielectric properties. From the measurement of optical responses using a triangular voltage wave, it was found that the phase in which the transmission intensity indicated four stable states was the $S^*_{C_\gamma}$ phase. The T–E phase diagram was obtained on the basis of apparent tilt angle measurements. It was confirmed that the $S^*_{C_\gamma}$ phase appeared after a single application of the field. In a thin cell ($< 3\ \mu$m), the transition between bistable states and that between three stable states in apparent tilt angle were simultaneously observed at the same temperature. The ratio

of the area of three stable regions to that of bistable regions gradually changed with temperature in the wide temperature range. It was found that in the thin cell the S_C^* phase completely disappeared and the coexistence of ferroelectric and antiferroelectric phases was observed. In the polarizing microscopic observation, a characteristic texture in which focal-conics were periodically aligned parallel to the layer was observed. These periodically aligned focal-conics appeared at the boundary between ferroelectric and antiferroelectric domains and remained in the complete antiferroelectric phase. The movement of the zig–zag defect caused by the application of the voltage was also observed.

References

[1] MEYER, R. B., LIEBERT, L., STRZELECKI, L., and KELLER, P., 1975, *J. Phys., Paris*, **36,** L69.

[2] GOODBY, J. W., BLINC, R., CLARK, N. A., LAGERWALL, S. T., OSIPOV, M. A., PIKIN, S. A., SAKURAI, T., YOSHINO, K., and ZEKS, B., 1991, *Ferroelectric Liquid Crystals* (Gordon & Breach).

[3] OZAKI, M., YOSHINO, K., SAKURAI, T., MIKAMI, N., and HIGUCHI, R., 1987, *J. chem. Phys.*, **86,** 3648.

[4] MIKAMI, N., HIGUCHI, R., SAKURAI, T., OZAKI, M., and YOSHINO, K., 1986, *Jap. J. appl. Phys.*, **25,** L833.

[5] YOSHINO, K., OZAKI, M., TANIGUCHI, H., ITO, M., SATOH, K., YAMASAKI, N., and KITAZUME, T., 1987, *Jap. J. appl. Phys.*, **26,** L77.

[6] TANIGUCHI, H., OZAKI, M., YOSHINO, K., SATOH, K., and YAMASAKI, N., 1988, *Ferroelectrics*, **77,** 137.

[7] TANIGUCHI, H., OZAKI, M., TOSHIMA, K., SATOH, K., and YAMASAKI, N., 1988, *Ferroelectrics*, **77,** 131.

[8] YOSHINO, K., TANIGUCHI, H., and OZAKI, M., 1989, *Ferroelectrics*, **91,** 267.

[9] OZAKI. M., HATAI, T., TAGAWA, A., NAKAO, K., TANIGUCHI, H., and YOSHINO, K., 1989, *Jap. J. appl. Phys.*, **28,** Suppl. 28–2, p. 130.

[10] CHANDANI, A. D. L., HAGIWARA, T., SUZUKI, Y., OUCHI, Y., TAKEZOE, H., and FUKUDA, A., 1988, *Jap. J. appl. Phys.*, **27,** L729.

[11] CHANDANI, A. D. L., GORECKA, E., OUCHI, Y., TAKEZOE, H., and FUKUDA, A., 1989, *Jap. J. appl. Phys.*, **28,** L1265.

[12] GORECKA, E., CHANDANI, A. D. L., OUCHI, Y., TAKEZOE, H., and FUKUDA, A., 1990, *Jap. J. appl. Phys.*, **29,** 131.

[13] ORIHARA, H., FUJIKAWA, T., ISHIBASHI, Y., YAMADA, Y., YAMAMOTO, N., MORI, K., NAKAMURA, K., SUZUKI, Y., HAGIWARA, T., and KAWAMURA, I., 1990, *Jap. J. appl. Phys.*, **29,** L333.

[14] YAMADA, Y., YAMAMOTO, N., MORI, K., NAKAMURA, K., HAGIWARA, T., SUZUKI, Y., KAWAMURA, I., ORIHARA, H., and ISHIBASHI, Y., 1990, *Jap. J. appl. Phys.*, **29,** 1757.

[15] MORITAKE, H., TAGAWA, A., OZAKI, M., and YOSHINO, K., 1991, *Jap. J. appl. Phys.*, **30,** 2377.

[16] YOSHINO, K., NAKAO, K., TANIGUCHI, H., and OZAKI, M., 1987, *J. phys. Soc. Japan*, **56,** 4150.

[17] HIRAOKA, K., CHANDANI, A. D. L., GORECKA, E., OUCHI, Y., TAKEZOE, H., and FUKUDA, A., 1990, *Jap. J. appl. Phys.*, **29,** 1473.

[18] OKABE, N., SUZUKI, Y., KAWAMURA, I., ISOZAKI, T., TAKEZOE, H., and FUKUDA, A., 1992, *Jap. J. appl. Phys.*, **31,** L793.

[19] CHANDANI, A. D. L., OUCHI, Y., TAKEZOE, H., FUKUDA, A., TERASHIMA, K., FURUKAWA, K., and KISHI, A., 1989, *Jap. J. appl. Phys.*, **28,** L1261.

[20] RIEKER, T. P., CLARK, N. A., SMITH, G. S., PARMAR, D. S., SIROTA, E. B., and SAFINYA, C. R., 1987, *Phys. Rev. Lett.*, **59,** 2658.

[21] OUCHI, Y., TAKANO, H., TAKEZOE, H., and FUKUDA, A., 1988, *Jap. J. appl. Phys.*, **27,** 1.